Earthq Eng & Eng Vib (2017) 16: 415-433 **DOI**:10.1007/s11803-017-0390-0

Rapid repair techniques for severely earthquake-damaged circular bridge piers with flexural failure mode

Sun Zhiguo[1†], Li Hongnan[2‡], Bi Kaiming[3†], Si Bingjun[2‡] and Wang Dongsheng[4‡]

1. *Department of Disaster Prevention Engineering, Institute of Disaster Prevention, Beijing 101601, China*
2. *Faculty of Infrastructure Engineering, Dalian University of Technology, Dalian 116024, China*
3. *Centre for Infrastructural Monitoring and Protection, School of Civil and Mechanical Engineering, Curtin University, Kent Street, Bentley, WA 6102, Australia*
4. *Institute of Road and Bridge Engineering, Dalian Maritime University, Dalian 116026, China*

Abstract: In this study, three rapid repair techniques are proposed to retrofit circular bridge piers that are severely damaged by the flexural failure mode in major earthquakes. The quasi-static tests on three 1:2.5 scaled circular pier specimens are conducted to evaluate the efficiency of the proposed repair techniques. For the purpose of rapid repair, the repair procedure for all the specimens is conducted within four days, and the behavior of the repaired specimens is evaluated and compared with the original ones. A finite element model is developed to predict the cyclic behavior of the repaired specimens and the numerical results are compared with the test data. It is found that all the repaired specimens exhibit similar or larger lateral strength and deformation capacity than the original ones. The initial lateral stiffness of all the repaired specimens is lower than that of the original ones, while they show a higher lateral stiffness at the later stage of the test. No noticeable difference is observed for the energy dissipation capacity between the original and repaired pier specimens. It is suggested that the repair technique using the early-strength concrete jacket confined by carbon fiber reinforced polymer (CFRP) sheets can be an optimal method for the rapid repair of severely earthquake-damaged circular bridge piers with flexural failure mode.

Keywords: rapid repair; severely earthquake-damaged; circular bridge piers; flexural failure mode; CFRP; early-strength concrete

1 Introduction

Reinforced concrete (RC) bridges are key components in the transportation network and will provide immediate emergency services following an earthquake event. It is of particular importance to ensure the seismic safety of bridge structures during severe earthquakes. It was repeatedly observed in previous major earthquakes that seismic induced damage to bridge structures was mainly on the bridge piers, which may experience inelastic deformation or even collapse during strong earthquakes. Restoration of these damaged bridge piers to serviceable condition may take a long time and therefore delay the rescue process. If these damaged bridge piers could be repaired and rehabilitated rapidly, it would be economical than having to demolish and reconstruct them. Also, rapidly repaired piers would greatly facilitate the rescue process and save more lives.

Recently, an increasing amount of research is becoming available on the feasibility of repair techniques for RC columns or bridge piers. Concrete jacketing (Fukuyama *et al*., 2000; Lehman *et al*., 2001), steel jacketing (Frangou *et al*., 1995; Aboutaha *et al*., 1999; Youm *et al*., 2006; Fakharifar *et al*., 2015) and fiber reinforced polymer (FRP) wrapping (Saadatmanesh *et al*., 1997; Xiao and Ma, 1997; Li and Sung, 2003; Chang *et al*., 2004; Rutledge *et al*., 2014; Yang *et al*., 2015a; 2015b) have been proven to be effective for repairing earthquake-damaged RC columns or bridge piers. Different repair techniques for RC columns or piers that failed in flexural (Lehman *et al*., 2001; Chang *et al*., 2004; Youm *et al*., 2006; Shin and Andrawes, 2011; He *et al*., 2013a; Rutledge *et al*., 2014), shear (Fukuyama *et al*., 2000; Li and Sung, 2003; Sun *et al*., 2011; Lavorato and Nuti, 2015) and lap splice failure modes (Saadatmanesh *et al*., 1997; Xiao and Ma, 1997; Aboutaha *et al*., 1999; Kim and Choi, 2010) were proposed and evaluated by experimental studies. Moreover, some techniques for

Correspondence to: Sun Zhiguo, Department of Disaster Prevention Engineering, Institute of Disaster Prevention, Beijing, 101601, China
Tel: +86 18941134800
E-mail: szg_1999_1999@163.com
†Associate Professor; ‡Professor

Supported by: National Natural Science Foundation of China under Grant No. 51678150; Science for Earthquake Resilience under Grant No. XH17064; and Australian Research Council Discovery Early Career Researcher Award (DECRA)
Received September 16, 2015; **Accepted** January 23, 2016

repairing earthquake-damaged RC columns or bridge piers have been used in engineering practice. For example, following the 1995 Kobe earthquake in Japan, many kinds of manuals and guidelines for repairing earthquake-damaged RC buildings were proposed, and repair techniques using steel jacketing, grouting mortar, and/or additional bars have been adopted for actual repair or strengthening (Fukuyama *et al*., 2000). During the 2008 Wenchuan earthquake in China, four bridge piers in the Huilan interchange were severely damaged and many other piers suffered from minor-to-moderate damage (Sun *et al.*, 2012). The damaged piers were repaired by steel jacketing and grouting mortar (Wang, 2010). Relatively little research (Cheng *et al*., 2003; Sun *et al*., 2011; Shin and Andrawes, 2011; He *et al*., 2013a, 2013b; Vosooghi and Saiidi, 2013a, 2013b; Lavorato and Nuti, 2015), however, has focused on the rapid repair technique for severely earthquake-damaged bridge piers. This technique was not emphasized and timely reopening of bridges was not a consideration among most of the previous studies. Therefore, new techniques are needed to effectively and rapidly restore the performance of these damaged bridge piers.

Sun *et al*. (2011) proposed a rapid repair technique for severely earthquake-damaged bridge piers with a flexural-shear failure mode by using early-strength concrete and carbon fiber reinforced polymer (CFRP) sheets. Quasi-static testing results of six circular pier specimens has shown that the damaged pier specimens with the flexural-shear failure mode could be repaired within four days, and the repaired specimens exhibited both higher strength and deformation capacity than the original ones. Note that all the original specimens failed with a flexural-shear mode in the tests, and the CFRP sheets were used around the full height of the specimens. The proposed method may not be effective if the bridge piers fail with a flexural mode.

Shin and Andrawes (2011) proposed a rapid repair technique for the emergency repair of severely earthquake-damaged RC columns by using spiral bars made of shape memory alloys (SMAs). The repair of each column was conducted within 15 hours, and the repaired columns were tested 24 hours after starting of the repair process. The quasi-static tests on two columns showed that the proposed repair technique was successful in fully restoring the lateral strength, stiffness, and ductility of the columns. However, one limitation of this technique is that the SMA is expensive for engineering practice. Also, in order to provide an active confinement for concrete, the SMA spiral bars have to be heated using a fire torch, which is not easy to be applied in engineering practice.

A technique for the rapid repair of severely earthquake-damaged RC columns with externally bonded CFRP was developed by He *et al*. (2013a). Three severely damaged square RC columns with buckled or fractured longitudinal bars were repaired within four or five days. Results indicated that the technique was successful in restoring the strength of the columns without the fractured longitudinal bars, but only partially successful for the column with fractured longitudinal bars located near the column base. He *et al*. (2013b) also presented the results of tests for evaluating the effectiveness of a rapid repair method (three days) by using quickset repair mortar and externally bonded CFRP. The tests were conducted with five severely damaged square RC columns with different damage conditions due to different loading combinations of bending, shear and torsion. It was concluded that the technique could be successful for severely damaged columns with damage to the concrete and transverse bars. Note that these studies only focused on the RC columns with square section.

A rapid and effective repair method for earthquake-damaged circular RC bridge piers by using CFRP was developed by Vosooghi and Saiidi (2013a, 2013b). Based on analyses of shaking table testing results, repair design guidelines for the piers were developed to determine the needed number of CFRP layers. It was concluded that when no longitudinal bar rupture, bar splice or shear failure occurred in the bridge pier, this method can be applied successfully, which means it can be used for rapid repair of bridge piers with minor to moderate damage. Moreover, the accelerated curing techniques utilized in their study (in order to reduce the repair time) are mostly feasible in the laboratory environment and would be difficult to be applied in real engineering practice.

Longitudinal bar fracture damage may occur for piers under a strong earthquake. Rapid repair techniques for replacement of the damaged longitudinal bars were proposed by Cheng *et al*. (2003) and Lavorato and Nuti (2015). For restoration of hollow bridge piers after an earthquake, Cheng *et al*. (2003) proposed a rapid repair technique by using dog-bone shape bars and FRP wraps. The dog-bone shape bars were used to replace the fractured longitudinal bars in the plastic hinges and FRP wraps were used to enhance the deformation of the piers. The proposed repair procedure could be completed within one week, and the effectiveness of the technique was verified by quasi-static tests. Lavorato and Nuti (2015) recently proposed a rapid repair technique for severely earthquake-damaged bridge piers by using epoxy adhesive, stainless steel rebar, self-compacting concrete and CFRP wrapping. The stainless steel rebar was used to replace the damaged part of the original bar, and the CFRP wrapping was used to improve the shear strength and ductility of the specimen. The effectiveness of the repair technique was assessed by pseudo-dynamic tests.

Based on the current seismic design criteria, RC bridge piers are designed to allow some nonlinear behavior such as the undergoing concrete cracking, concrete cover and concrete core spalling, and longitudinal bar bucking damage to provide a significant rotation capacity at the plastic hinge regions without

collapse. This damage can be classified as flexural failure, and most existing bridge piers would fail in this mode. Thus, it is urgent and important to develop a rapid repair technique for these bridge piers.

The main objective of the present study is to develop a rapid repair technique for severely earthquake-damaged bridge piers with a flexural failure mode by using available construction materials. To fulfill this objective, experimental investigations are undertaken on three severely earthquake-damaged bridge piers by using early-strength concrete, additional longitudinal bars, epoxy and CFRP sheets. First, three circular original pier specimens are designed and severely damaged under cyclic lateral force and constant axial load. Then, the damaged specimens are repaired by using three different techniques which will be discussed in Section 2.4. For the purpose of rapid repair, the entire repair work for each specimen takes approximately three days. On the fourth day, the repaired specimens are retested to evaluate the effectiveness of different repair techniques. The performance of the repaired specimens is evaluated by comparing them with the corresponding original ones. A preliminary introduction of the experimental study has been shown elsewhere by Si *et al.* (2010), a more detailed description of the experimental results is provided in the present study. Moreover, the design equation for the needed CFRP thickness proposed by Vosooghi and Saiidi (2013b) is evaluated by using the available test data. Finally, a model to predict the cyclic behavior of the repaired pier specimens is developed.

The techniques proposed in the present study should have three features which are different from other repair techniques. First, the techniques can be labelled as "rapid," which entail the piers to be repaired within a few days. Second, the techniques are effective for restoring the behavior of "severely" damaged bridge piers. Finally, the operation procedure of the techniques is relatively simply and can be conveniently applied in engineering practice. Moreover, the techniques may have to be viewed as "temporary" for the emergency response after an earthquake as the long-term durability of the repaired specimens is not yet well understood.

2 Experimental study

2.1 Original pier design

A direct displacement based seismic design procedure for RC bridge piers was proposed based on the improved capacity spectrum method by Wang *et al*. (2006). A total of three prototype bridge piers were designed to illustrate the design procedure. Among the three prototype members, two piers were designed based on the displacement criteria representing newly built bridge piers and the other one was based on strength criteria representing commonly used bridge piers in China. The piers designed based on displacement criteria were expected to behave in a ductile manner to avoid collapse under a strong earthquake with peak ground acceleration (PGA) of about 0.8 g. The piers were designed with adequate transverse reinforcement and the strength demand could be reduced by using a low longitudinal reinforcement ratio. For the pier designed based on strength criteria, more longitudinal reinforcements were used to increase the lateral strength. The pier was expected to behave in the elastic range under a minor earthquake with PGA of about 0.14 g, while the behavior of the pier under a strong earthquake was not clear. All the prototype piers had a circular section with a diameter of 1000 mm, and the height of all the piers was 6000 mm. The concrete compression strength used in the prototype piers was about 30 MPa, and the axial load ratio of the piers under the dead load was about 0.14, which was within the range for commonly used bridge piers in China. Chinese Grade HRB 335 and HPB 235 reinforcement bars were used as longitudinal and spiral bars, respectively.

All three prototype piers are used to guide the design of the original pier specimens in the present study. Three original pier specimens are designed and designated as A10, A12 and A14, respectively. A scale factor of 1/2.5 is selected based on the capacity limitation of the test setup. Note that previous studies (Lu *et al*. 1999; Ozcelik *et al*., 2011) have shown that such scaled RC specimens can represent the expected load deformation response of the corresponding full scale members if some measures are followed in selecting the specimen dimension and material properties. In the design of the original pier specimens, the dimension of the specimens is scaled following the scale factor of 1/2.5. The other parameters of the specimens, such as the longitudinal and transverse reinforcement ratios, the axial load ratio, the concrete compression strength, and the grade of the longitudinal and transverse bars, are kept the same with the prototype piers.

The details of original pier specimens are shown in Fig. 1 and their parameters are listed in Table 1. All the specimens have a circular section with a diameter of 400 mm and with a heavy RC footing. The footing, which is fixed to the test platform, is strong enough to provide a fixed end for the specimen. The height of the specimens measured from the top surface of the footing to the point where the lateral load is applied is 2400 mm, which corresponds to an aspect ratio of 6.0.

All the specimens are reinforced with 24 longitudinal bars evenly distributed around the perimeter of the section. The longitudinal bars for all the specimens are deformed bars specified as Grade HRB 335 in China. For the specimen A10, longitudinal bars with 10 mm diameter are used, resulting in a longitudinal reinforcement ratio of 1.5%. For the specimens A12 and A14, longitudinal bars with diameters of 12 and 14 mm are used respectively, and the longitudinal reinforcement ratios become 2.2% and 2.9%. Note that the 2008 seismic design code for highway bridges

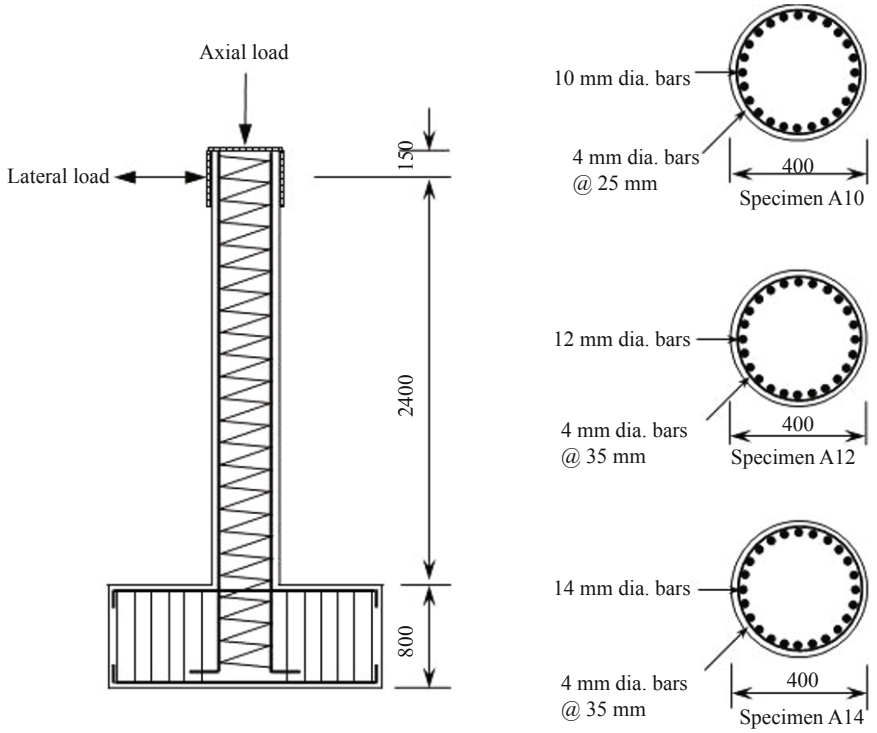

Fig. 1 Details of original pier specimens (unit: mm)

Table 1 Summary of design details of original pier specimens

Specimen	f_c' (MPa)	Longitudinal bars		Spiral bars			Axial load ratio
		d_b (mm)	ρ_l (%)	d_s (mm)	s (mm)	ρ_s (%)	$P/A_g f_c'$
A10	31	10	1.5	4	25	0.54	0.15
A12	31	12	2.2	4	35	0.40	0.14
A14	31	14	2.9	4	35	0.40	0.13

Note: f_c' is the concrete compressive strength, d_b is the longitudinal bar diameter, ρ_l is the longitudinal reinforcement ratio, d_s is the spiral bar diameter, s is the spacing of spiral bar, ρ_s is the volumetric transverse reinforcement ratio, P is the applied axial load, and A_g is the gross area of the pier section.

in China (JTG/T B02-01 2008) stipulates the minimum longitudinal reinforcement ratio for bridge piers to be 0.6%. The longitudinal reinforcement ratios used in the present study are well above the minimum requirement.

For all three specimens, Chinese Grade HPB 235 smooth bars with a diameter of 4 mm are used as the spiral bars. For the specimen A10, the spiral bars are spaced at a distance of 25 mm, resulting in a volumetric transverse reinforcement ratio of 0.54%. For the specimens A12 and A14, the spacing is 35 mm and the volumetric transverse reinforcement ratio changes to be 0.4% for both of the specimens. Note that the minimum volumetric transverse reinforcement ratio specified in the 2008 seismic design code for highway bridges in China is 0.4% (JTG/T B02-01 2008), and the amount of spiral reinforcement in all the three specimens meet the requirement specified by this code.

The specimens A10 and A12 are selected to represent the bridge piers designed based on the displacement criteria, and specimen A14 is selected to represent piers designed based on the strength criteria. As a result, specimen A10 is designed with the minimum longitudinal reinforcement ratio, while adequate transverse reinforcement bars are used to ensure the ductility of the specimen. Specimen A14 is designed with the maximum longitudinal reinforcement ratio to ensure the lateral strength of the specimen. For specimen A12, the transverse reinforcement ratio is equal to specimen A14, and the longitudinal reinforcement ratio for this specimen is between the values for specimens A10 and A14.

Before the test, all the important parameters related to the specimens are tested and measured. For example, the average concrete compressive strength is measured as 31 MPa by using 150 mm × 150 mm × 300 mm prism specimens. The yielding strengths of the 10 mm, 12 mm and 14 mm diameter reinforcement bars are 362, 367 and 399 MPa, respectively. The 4 mm spiral bars of all the specimens have a yielding strength of 273 MPa. The axial load ratios of the specimens are between 0.13 and 0.15, as shown in Table 1.

2.2 Test setup and loading sequence

The test procedures for the original and repaired

pier specimens are similar. All the specimens are tested under lateral cyclic loadings while simultaneously being subjected to a constant axial load. The test setup for each specimen is shown in Fig. 2, in which the specimen is vertically fixed to the strong floor in the laboratory and a steel reaction frame is used to provide the axial and cyclic lateral loads. At the top of the specimen, a vertical hydraulic actuator is used to provide the axial load, which is used to simulate the weight of the bridge superstructure. The vertical actuator is connected to the reaction frame by a rolling shaft, in which a series of rollers are provided to allow free sliding of the specimen top in the lateral direction. The rolling shaft guarantees no interference between the test setup and deformation of the specimen. Under the vertical actuator, the specimen is loaded by two horizontal actuators to provide the lateral cyclic loads. Note that the horizontal actuators could only provide compressive force, but are not able to provide tensile force. Two horizontal actuators are used together to provide the cyclic lateral loads.

The lateral loading history presented in Fig. 3 is applied to each original specimen. The loading cycles are divided into two phases: the load control phase and the displacement control phase. The load control is used to define the specimen's experimental yield displacement Δ_{ey}. Then, a displacement control loading sequence is used. The displacement controlled loading history includes five complete cycles for $u_{e\Delta}$ = 1, 2, 3,……, until the lateral strength of the specimen declines to 80% of the peak loads. Here, $u_{e\Delta}$ is the ratio of the lateral displacement Δ to the experimental yield displacement Δ_{ey}. The definition of the experimental yield displacement Δ_{ey}, is shown in Fig. 3(a), where F_{ty} is the specimen's theoretical yield strength, which can be calculated based on the fiber element model and measured material properties. During the tests, the experimental yielding displacement Δ_{ey} for specimen A10 is defined as 15 mm, and 20 mm is used as the experimental yielding displacement for specimens A12 and A14. Note that $5\Delta_{ey}$ (75 mm) displacement cycles have not been applied to specimen A10 as a result of equipment error, after the $4\Delta_{ey}$ (60 mm) displacement cycles, $6\Delta_{ey}$ (90 mm) displacement cycles are applied.

For the repaired pier specimens, since the lateral stiffness may be different from that of the companion original ones, for comparison purposes, the repaired specimens are subjected to the same lateral displacement history as those of the original ones.

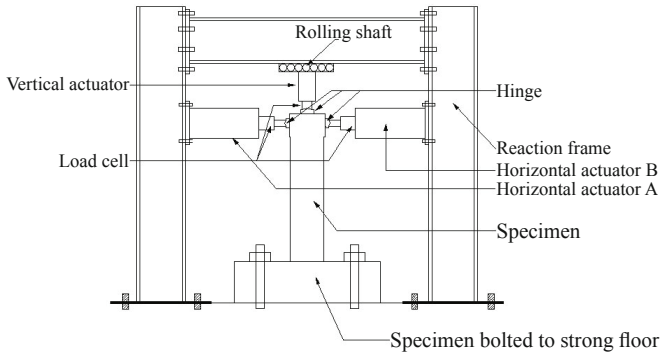

Fig. 2 Test setup

2.3 Damage patterns of original specimens

All the specimens have been tested to failure, as indicated by a strength reduction exceeding 20% with severe damage. The experimental results exhibit the flexural failure mode in regions close to the bottom of the specimens (the plastic hinge regions). The observed damage includes concrete cracking, concrete cover and concrete core spalling, spiral bar fracture and apparent longitudinal bar buckling.

Table 2 summarizes the damage details of original pier specimens before repair. It is observed that the concrete spalling damage concentrated at the specimen bottom and the spalling heights vary from 250 to 315 mm, corresponding to 0.6 to 0.8 times of the section depth. The maximum concrete crushing depths are between 45 and 52 mm, which are larger than 1/10 of the section depth. Although no longitudinal bar fracturing damage

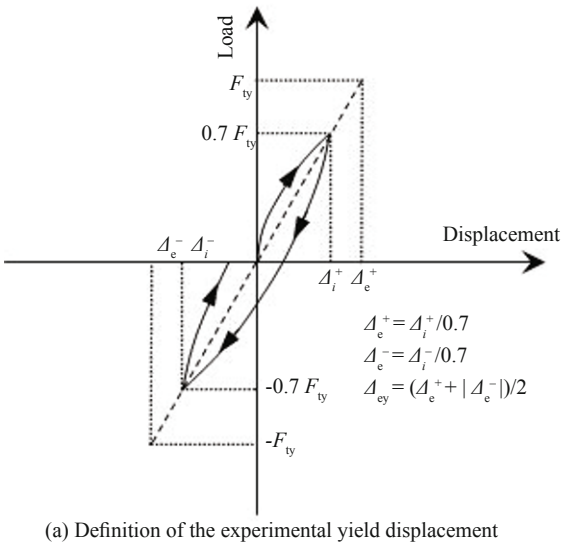

(a) Definition of the experimental yield displacement

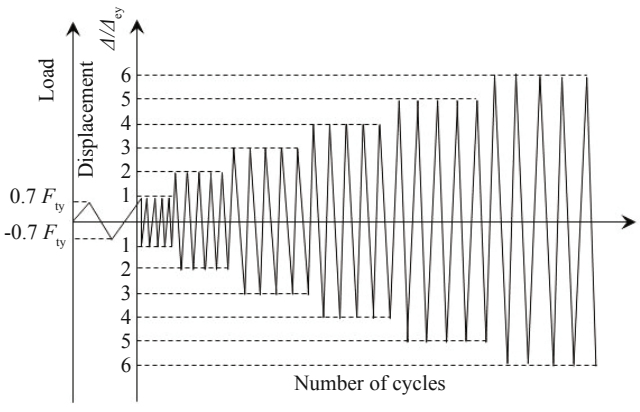

(b) Lateral loading sequence

Fig. 3 Lateral loading sequence of original pier specimens

Table 2 Pier damage observation

Specimen	Concrete damage		Reinforcing bar damage	
	Spalling height (mm)	Concrete crushing depth (mm)	No. of buckled longitudinal bars	No. of fractured spiral bars
A10	270	45	10	0
A12	250	50	10	2
A14	315	52	14	0

is observed, the number of buckled longitudinal bars are 10 and 14 for each specimen, indicating that more than 40% of the longitudinal bars are severely damaged. Additionally, two spiral bars in specimen A12 are fractured, while no fracturing damage of spiral bars is observed in other specimens. Note also that horizontal flexural concrete cracking damage occurs up to a height of 1600 mm for all the specimens after the original test, indicating that about 2/3 of the height of all the specimens suffer concrete cracking damage.

According to a previous study by Lehman *et al*. (2001), any visible evidence of concrete core crushing, longitudinal bar buckling, or longitudinal/transverse bar fracture was classified as severe damage. Also, damage can be classified as "local failure/collapse" level if the buckling of the longitudinal bar, rupture of the transverse bar, or concrete core crushing was observed for bridge components as defined by Hose *et al*. (2000), and usually this type of damaged components should be replaced and no effective repair techniques were available. Based on these classifications, all the damaged specimens here could be classified as severely damaged bridge piers. In contrast to the common suggestion, new rapid repair techniques for these specimens are proposed and experimentally investigated in the present study.

Figure 4 shows the detailed damage to the original pier specimens. The damaged specimens are pushed back to the original position (zero lateral displacement) before the repair operation begins.

2.4 Pier repair

In order to develop a rapid and effective repair technique for the severely earthquake-damaged bridge piers, three different design philosophies, which involve three different repair techniques, are proposed and evaluated herein.

For the damaged specimen A10, it is intended to repair the specimen by plastic hinge relocation. By using this repair philosophy, the damaged part (the plastic hinge region) would be repaired by involving a strong jacket and the new plastic hinge would be formed to occur just above the jacket. To achieve this, some design objectives must be considered. First, the flexural strength of the new plastic hinge should be reduced so that the shear demand does not exceed the shear capacity of the specimen. This is the reason why the specimen A10 (with the maximum transverse reinforcement ratio and the minimum longitudinal reinforcement ratio) is selected to be repaired by using this philosophy. Second, the strength of the repaired region should be large enough so that the plastic hinge would not occur there again. This design philosophy was adopted by Lehman *et al*. (2001) and Rutledge *et al*. (2014) for the repair of severely earthquake-damaged bridge piers.

For the damaged specimen A12, it is also intended to repair the specimen by plastic hinge relocation (test

(a) Specimen A10

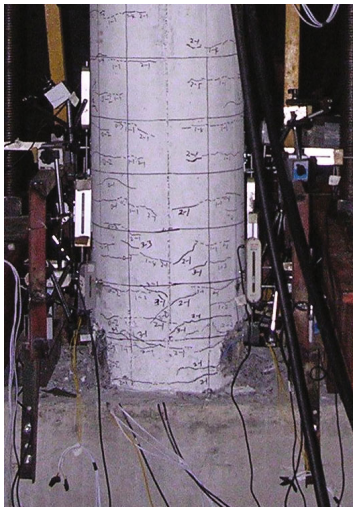

(b) Specimen A12

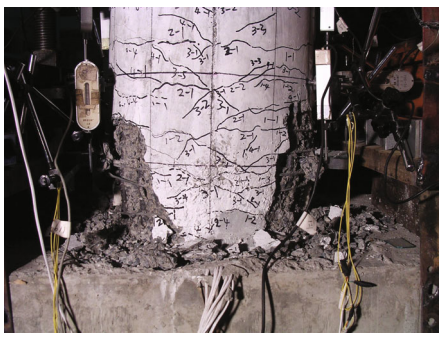

(c) Specimen A14

Fig. 4 Damage states of original pier specimens

results indicate that the repair technique for this specimen failed, which will be discussed in the following section). The repair technique of concrete jacketing is adopted for this specimen. Note that Júlio *et al*., (2005) and Julio and Branco (2008) conducted monotonic and quasi-static tests for RC columns strengthened by RC jackets. The results revealed that for undamaged columns with an aspect ratio larger than 1.0, it is not necessary to consider any type of interface treatment before casting a RC jacket with a thickness less than 17.5% of the column width to obtain a monolithic behavior of the retrofitted specimen. For specimen A12, early-strength concrete jacket and additional longitudinal bars are used to repair the damaged region with no special interface treatment between the old and new concrete. This repair technique is used to evaluate the collaboration between the section of the jacket and the original damaged pier section.

For the damaged specimen A14, it is intended that the plastic hinge would occur at the repaired region. By using this repair philosophy, the damage to the repaired specimen should concentrate in the repaired region, while no obvious damage would occur above the repaired region. To achieve this, the flexural strength of the repaired region should be less than or equal to the sections above the repaired region. The repair technique by concrete jacketing is also adopted for this specimen. Note that additional longitudinal bars are used to repair both damaged specimens A10 and A12. However, it is difficult to anchor new bars in the foundation of a real pier with a high longitudinal reinforcement ratio. The reason is that the longitudinal bars are very congested. Also, the anchor of new longitudinal bars would cause harm to the other bars in the anchorage area. As a result, additional longitudinal bars are not used to repair the damaged specimen A14 (with the maximum longitudinal reinforcement ratio in the present study). An early-strength concrete jacket is used and wrapped with CFRP sheets to provide lateral confinement for the repaired region.

Before repairing the damaged specimen, the loose concrete in and around the plastic hinge region is removed, and the buckled longitudinal bars are straightened as much as possible. Subsequently, the specimens are repaired using three different techniques, and the details are depicted in Fig. 5 and illustrated as follows.

For specimen A10, eight additional longitudinal bars are first arranged outside the buckled longitudinal bars with an anchorage depth of 15 times their diameters (180 mm). The diameter of the additional bars is 12 mm, resulting in a total area of 904 mm^2, which is larger than the total area of the buckled longitudinal bars (ten 10 mm diameter bars with a total area of 785 mm^2). Before insertion of the additional bars, the holes, which were previously drilled into the footing, are injected with a two-component epoxy to ensure the bond strength between the bars and surrounding concrete. The anchorage depth l_d is selected based on the design code for strengthening concrete structures in China (GB 50367-2006) and compared with the value suggested by Yilmaz *et al*. (2013). The anchorage depth suggested by the GB 50367-2006 code is given as:

$$l_d = 0.2\alpha_{spt} d_b f_y / f_{bd} \quad (1)$$

where α_{spt} is the parameter to prevent concrete splitting failure and taken as 1.0 for the additional bar with a diameter less than 20 mm; d_b is the additional bar diameter; f_y is the yield strength of the additional bar, and f_{bd} is the shear bond strength of the epoxy. Equation (1) requires a length l_d of 176 mm for the additional bars used in the present study. Also, Yilmaz *et al*. (2013) suggested that

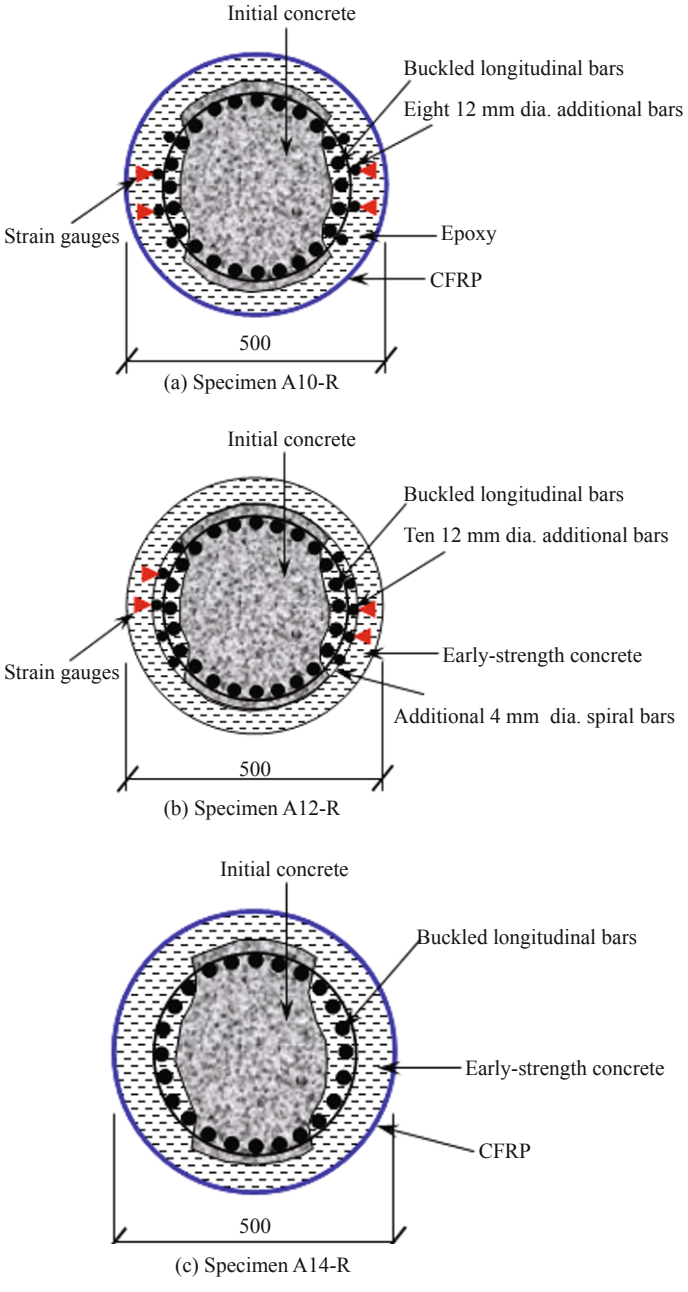

Fig. 5 Repair techniques for the damaged pier specimens

an anchorage depth of 15 times the anchor bar diameter should be required to obtain a ductile tensile failure for post-installed chemical anchors embedded in low strength concrete. As a result, 15 times of additional bar diameter (180 mm) is selected for the anchorage depth herein. After that, a circular steel wrap with a diameter of 500 mm is provided as the form board and the two-component epoxy (the same one that is used to anchor the additional bars) is injected between the original pier and steel wrap. Finally, the steel wrap is removed after 24 hours and the solidified epoxy is wrapped by two layers of CFRP sheets with the fiber orientated in the circumferential direction. The average thickness of a CFRP laminate used here is 0.111 mm with an elastic modulus of 245 GPa and an ultimate tensile strength of 3792 MPa along the fiber direction. The stress-strain relationship of the CFRP sheets is almost linear-elastic up to failure. The compressive and tensile strengths of solidified epoxy are 96 and 58 MPa, respectively. Both are much larger than the corresponding values of the original concrete. However, the compressive modulus of elasticity of the solidified epoxy is tested as 3088 MPa, which is much less than the original concrete.

For specimen A12, ten 12 mm diameter additional longitudinal bars are arranged outside the buckled longitudinal bars, all the bars are anchored into the RC footing, and the anchorage depth is selected to be the same as that in specimen A10. In order to ensure the flexural strength of the repaired specimen, the total area of the additional bars (1131 mm^2) is much larger that of the buckled longitudinal bars (785 mm^2). And the additional longitudinal bars are enclosed by 4 mm diameter spiral bars spaced at a distance of 25 mm. Next, a circular steel wrap with a diameter of 500 mm is provided as the form board. Early-strength concrete with a compressive strength of 30 MPa at three days is poured, and the form is removed once the repaired concrete is cured (only 24 h are needed). No adhesive or other interface treatment is used to bond the new concrete to the old concrete. The strength of the early-strength concrete is close to the original specimen to ensure that they are compatible.

Similar to specimen A12, the cross-section of specimen A14 is also enlarged by using the early-strength concrete with the same compression strength as used for specimen A12. However, no additional longitudinal bars are used for specimen A14. Similarly, no adhesive or other interface treatment is used between the old and new concrete. After it cures, the concrete surface is smoothed using sandpaper to prevent stress concentration in the CFRP sheets (Chang *et al*., 2004; He *et al*., 2013b; Vosooghi and Saiidi, 2013a). Finally, two layers of CFRP sheets with the fiber oriented in the circumferential direction are used to confine the concrete. The major steps of the repair procedures for all the specimens are shown in Fig. 6.

As illustrated in Table 1, the concrete spalling damage is concentrated at the bottom 250 to 315 mm of the specimens. To maximize the time efficiency, only the regions at and adjacent to the plastic hinge are repaired. As a result, the repair height for all the specimens is determined to be 450 mm. For the concrete cracking damage above the repaired region, as the residual concrete cracking width after unloading is very small and it is very difficult to inject epoxy successfully into the cracks, the concrete cracking damage above the repair height are not repaired. The repaired specimens are denoted with the extension "-R".

For the specimens A10-R and A12-R, four strain

(a) Specimen A10 after loose concrete removal

(b) Specimen A10 after installation of additional longitudinal bars

(c) Specimen A12 after additional longitudinal and spiral bars are arranged

(d) Specimen A14 before installation of the form board

(e) Specimen A14 after wrapping of CFRP

Fig. 6 Repair procedures of the specimens

gauges for each specimen are mounted on 4 additional longitudinal bars to measure the strains of the bars. The location of the strain gauges is shown in Figs. 5(a) and 5(b) with a height of 100 mm above the footing of the specimens. For specimens A10-R and A14-R, six strain gauges for each specimen are installed on the CFRP sheets to measure the strains in the circumferential direction at different loading levels, and the location of the strains is shown in Fig. 7.

The entire repair work of all the specimens spanned approximately three days. On the fourth day of the repair work, the repaired specimens were retested to evaluate the effectiveness of the three different repair techniques.

3 Test results of repaired specimens

3.1 Observed behavior

The following phenomena are observed for the repaired pier specimens. For specimen A10-R, no visible new damage is observed during the initial loading stage until the 30 mm ($2\Delta_{ey}$) displacement cycles. When the specimen is pushed to the pre-defined lateral displacements, the old cracks above the repaired region (not repaired during the repair process) re-open, but no visible cracks are observed in the repaired region. During the 45 mm ($3\Delta_{ey}$) displacement cycles, new flexural cracks are observed above the repaired region, and the width of new and old cracks increase with the top displacement. During the 60 mm ($4\Delta_{ey}$) displacement cycles, a new plastic hinge forms above the repaired region, concrete spalling and longitudinal bar buckling damage is observed just above the repaired region of the specimen. Note that the repaired region is so strong that no visible damage to the solidified epoxy and CFRP sheets is observed until completion of the test. Figure 8 shows the damage patterns of specimen A10-R.

For specimen A12-R, the damage is mainly concentrated at the repaired region. During the first lateral displacement cycle, vertical concrete cracks are observed in the concrete jacket. The reason for the premature vertical concrete cracks can be attributed to the high brittle behavior of the early-strength concrete without lateral confinement. Under a combined axial and horizontal load, the base section of the specimen expands laterally. As a result, vertical concrete cracks occur in the early-strength concrete. During the 40 mm ($2\Delta_{ey}$) displacement cycles, the maximum width of the vertical cracks in the concrete jacket reach 1.0 mm, and diagonal cracks are formed. During the 60 mm ($3\Delta_{ey}$) displacement cycles, the upper 30 cm part of the concrete jacket separates from the existing pier and the depth of the separated region increases during the next cycles. The new early-strength concrete jacket exhibits highly brittle behavior as lack of confinement. The concrete at the top of the jacketed region spalls off during the 80 mm ($4\Delta_{ey}$) displacement cycles, with the additional bars exposed. Figure 9 shows the damage patterns of specimen A12-R. Note also that all the additional longitudinal bars in specimens A10-R and A12-R perform well during the tests and no anchorage failure is observed.

For specimen A14-R, until the 40 mm ($2\Delta_{ey}$)

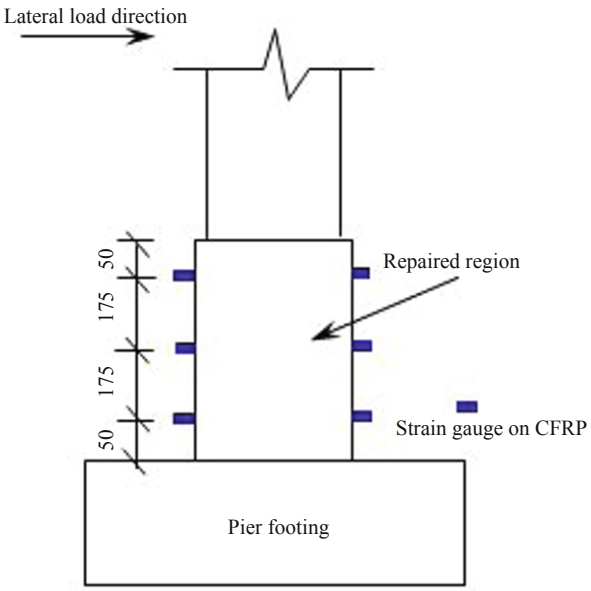

Fig. 7 Location of the strain gauges on the CFRP (Length unit: mm)

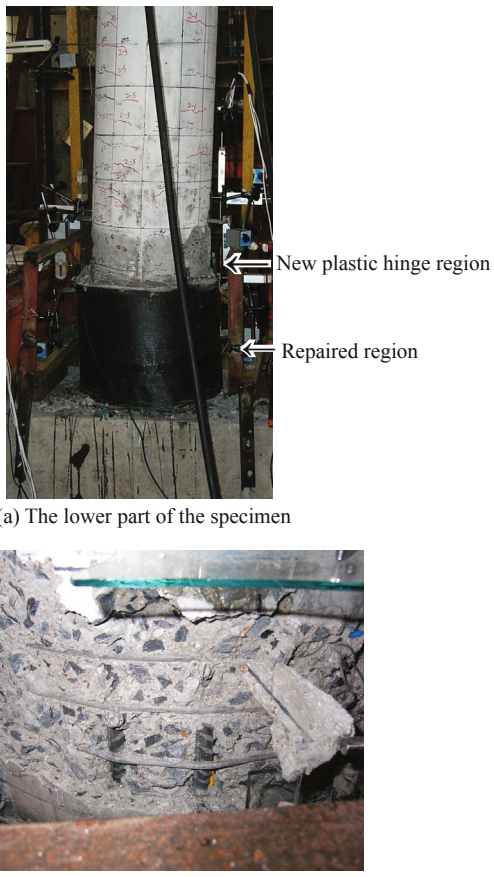

(a) The lower part of the specimen

(b) Concrete spalling and longitudinal bar bucking damages

Fig. 8 Damage patterns of Specimen A10-R

(a) Vertical and diagonal cracks of the concrete jacket

(b) Debonding failure between the concrete jacket and existing pier

(c) Spalling damage of the concrete jacket

Fig. 9 Damage patterns of Specimen A12-R

displacement cycles, the old concrete cracks above the repaired region re-open but no visible new damage is observed. During the 60 mm ($3\Delta_{ey}$) displacement cycles, new concrete cracks are observed above the repaired region, indicating that the repaired specimen has even larger lateral load carrying capacity compared to the original specimen. Also, flexural cracks on the CFRP sheets along the fiber direction are observed. At the end of the test, no apparent plastic hinge is formed and the failure pattern is dominated by the flexural cracks on the CFRP sheets along the fiber direction. Perhaps the concrete cracks are originally formed in the concrete, and the opening of these cracks result in splitting of the CFRP sheets. Note that no tension failure of the CFRP fibers is observed. The flexural cracking of the CFRP sheets is shown in Fig. 10.

3.2 Strength and deformation capacity

The measured lateral force (F)-displacement (Δ) hysteretic curves for the original and repaired pier specimens are shown in Fig. 11, and their skeleton curves are shown in Fig. 12. The measured maximum lateral strengths in both the positive and negative directions for the original and repaired specimens are indicated and listed in the skeleton curves.

As seen from Figs. 11 and 12, all the original pier specimens exhibit obvious lateral strength degradation during the maximum displacement cycles. No apparent reduction in the lateral strength is observed for all the repaired specimens, which indicates that these specimens exhibit larger deformation capacity than the original ones.

For specimen A10-R, as indicated in Figs. 11(a) and 12(a), the improvement in the lateral strength for the repaired specimen can be seen. The maximum lateral strength of the original specimen A10 is 75.0 kN in the positive direction and 80.0 kN in the negative direction, while those of the repaired specimen are 85.0 and 94.6 kN in those directions. The increase of lateral strength is attributed to the solidified epoxy. As shown in Fig. 8(a), the epoxy is so strong that a new flexural plastic hinge moves from the base of the pier to the portion just above the top of the repaired region. As a result, the effective height of the repaired specimen is reduced (changes from 2400 mm to 1950 mm) and leads to higher lateral strength of the repaired specimens. Note also that the measured maximum longitudinal strain in the additional longitudinal bars is about 0.00015, corresponding to a tensile stress of about 30 MPa, which is much less than the yield strength of the bar. This phenomenon can again be explained by the strong solidified epoxy. During the test, the epoxy is in the elastic range and the deformations are compatible between the additional longitudinal bar and surrounding epoxy. As the maximum measured tensile stress of the additional bar is much lower than the yield strength of the bar, it can be concluded that the additional bars did not play an obvious role in enhancing the behavior of the repaired specimen.

For specimen A12-R, as shown in Figs. 11(b) and 12(b), the measured maximum lateral strength of the

Fig. 10 Flexural cracks of CFRP sheets in specimen A14-R

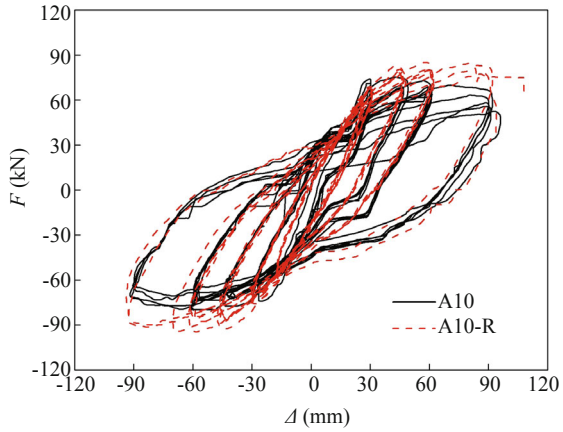

(a) Specimens A10 and A10-R

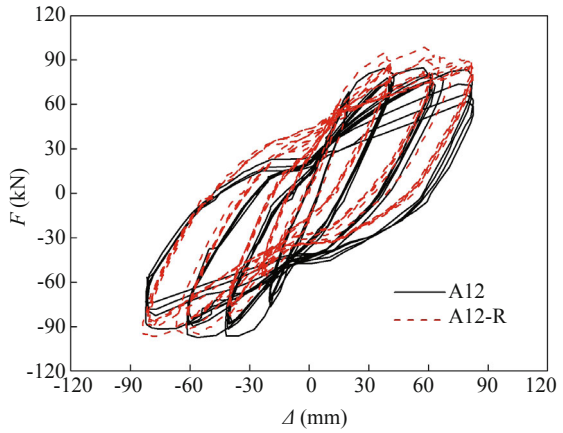

(b) Specimens A12 and A12-R

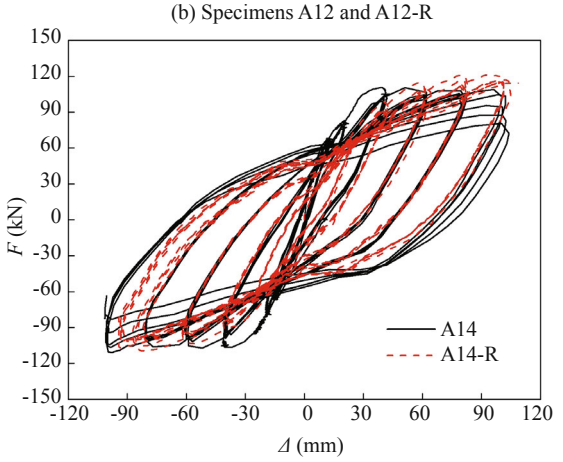

(c) Specimens A14 and A14-R

Fig. 11 The hysteretic curves of the specimens before and after repair

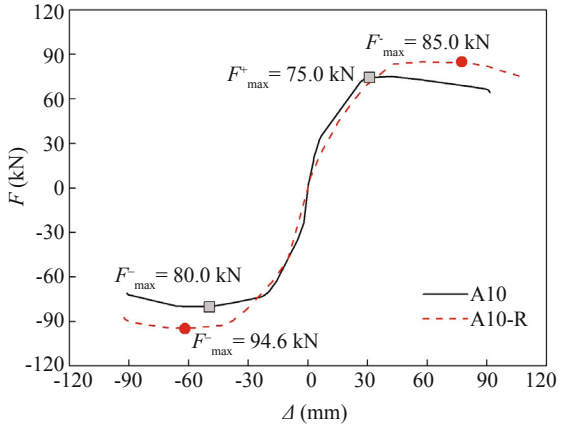

(a) Specimens A10 and A10-R

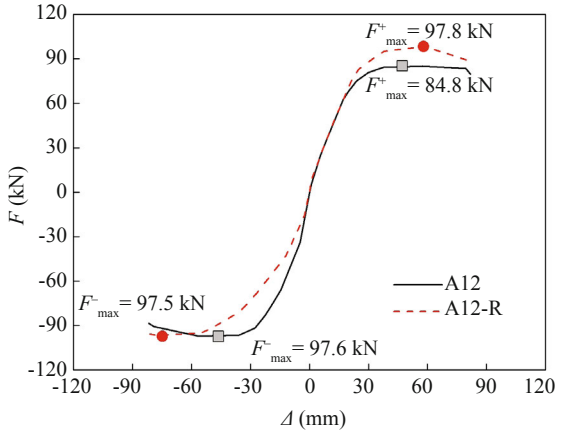

(b) Specimens A12 and A12-R

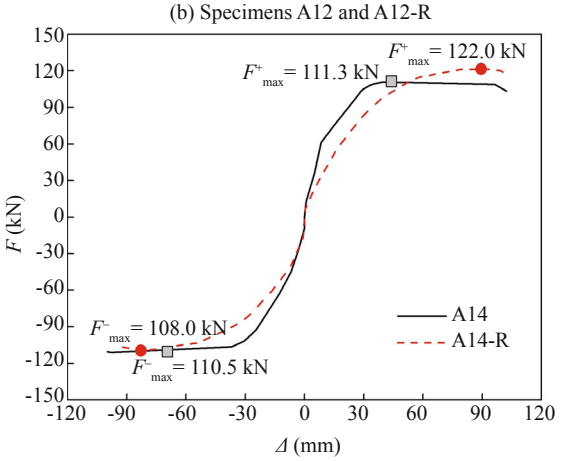

(c) Specimens A14 and A14-R

Fig. 12 The skeleton curves of the specimens before and after repair

repaired specimen is 1.15 times larger than that of the original one in the positive direction (97.8/84.8 = 1.15) and almost the same in the negative direction. It is seen that the lateral strength of the repaired specimen is slightly larger than the original one. Although the section of the repaired specimen is larger than that of the original one and many additional longitudinal bars are used, the brittle behavior of the concrete jacket and the debonding failure between the jacket and existing old concrete lead to a poor behavior of the repaired specimen. Note also that the measured maximum longitudinal strain in the additional longitudinal bars is about 0.0012, which is much less than their yield strain, indicating that the additional longitudinal bar did not play a role in restoring the behavior of the repaired specimen. The test results from this specimen indicate that the proposed repair technique using an early-strength concrete jacket and additional longitudinal bars is not satisfactory. The early-strength concrete jacket without FRP confinement or interface treatment is not recommended for repair of earthquake-damaged bridge piers.

For specimen A14-R, as indicated in Figs. 11(c) and 12(c), the repaired specimen has similar or even larger lateral load carrying capacity compared to the original one.

The maximum lateral strength of the original specimen A14 is 111.3 kN in the positive direction and 110.5 kN in a negative direction, while those of the repaired specimen are 122.0 kN and 108.8 kN in two different directions. Note that although no additional longitudinal bars are used in specimen A14-R, the lateral strength and deformation capacity of the repaired specimen are larger than that of the original one, which indicates that severely damaged circular bridge piers without fracture damage of longitudinal bars can be repaired successfully by using the concrete jacket and wrapped CFRP sheets. A similar conclusion was reported for square column specimens by He *et al*. (2013a; 2013b). As no additional bars are used, the repair process is easier and thus more feasible in engineering practice. The low cost of materials used, and the ease and speed of application, make the technique of using an early-strength concrete jacket wrapped with CFRP sheets very competitive for the rapid repair of damaged bridge piers.

3.3 Lateral stiffness of the specimens

The initial lateral stiffness K_1 of the specimens is calculated by using the slope of the linear part of the skeleton curves (taking the average value in both the positive and negative directions), and the values of the original and repaired specimens are shown in Fig. 13. It is seen that when compared with the original ones, all repaired specimens exhibit lower lateral stiffness during the initial lateral load stage. For specimens A10 and A10-R, the stiffness of the repaired specimen is slightly lower than that of the original one. This is because although the damage existed in the repaired specimen, the solidified epoxy in the repair region is very strong and the effective height of the repaired specimen is reduced, which increases the lateral stiffness of the pier. For specimens A12 and A12-R, the initial lateral stiffness of the original specimen is 5.37 kN/mm, and reduces to 3.56 kN/mm in the repaired specimen. This is because the concrete jacketing and additional bars did not play an obvious role in restoring the behavior of the repaired specimen. For specimens A14 and A14-R, the initial stiffness of the repaired specimen is 4.05 kN/mm, which is only 60% of that in the original specimen (6.70 kN/mm). This phenomenon is explained by the pre-existing damage in the repaired specimens, and the CFRP sheets wrapped in the circumferential direction had little influence on the lateral stiffness of the pier during the initial lateral load stage.

During the displacement control phase, the secant stiffness of the specimen K_Δ at the lateral displacement Δ is defined by the following equations:

$$K_\Delta = \frac{K_\Delta^+ + K_\Delta^-}{2} \tag{2}$$

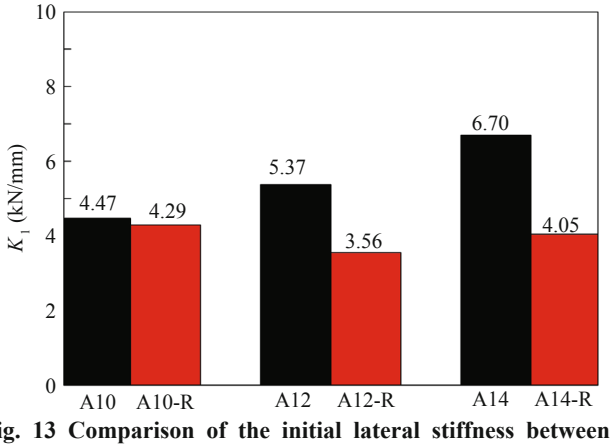

Fig. 13 Comparison of the initial lateral stiffness between original and repaired specimens

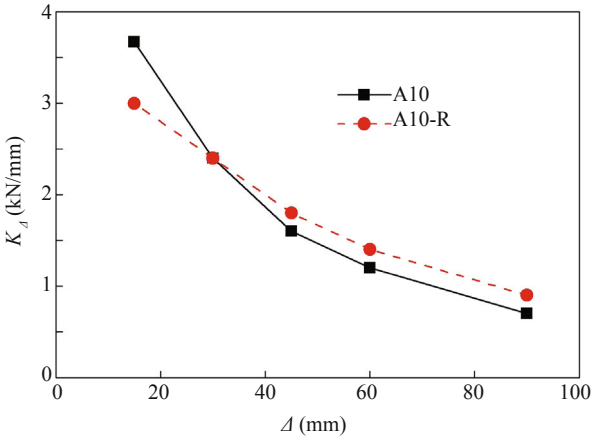

(a) Specimens A10 and A10-R

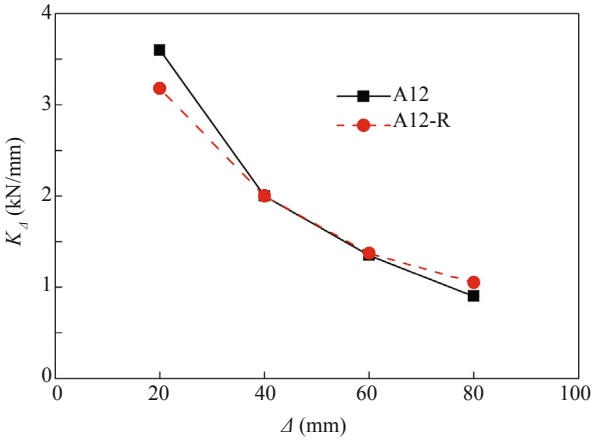

(b) Specimens A12 and A12-R

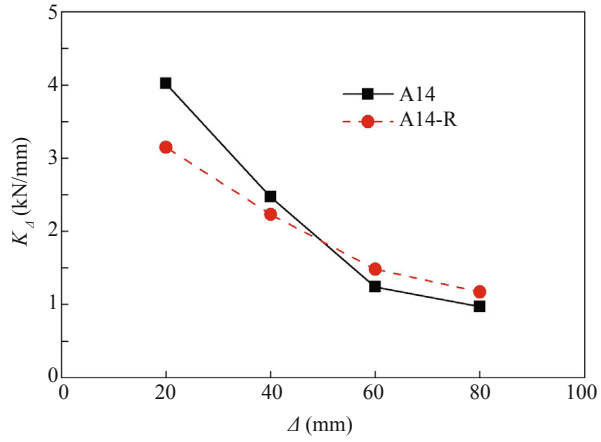

(c) Specimens A14 and A14-R

Fig. 14 Secant stiffness versus lateral displacement of the specimens

$$K_{\Delta}^{+}=\sum_{j=1}^{5}(F_{j,\max}^{+}/\Delta_{j,\max}^{+}),\ K_{\Delta}^{-}=\sum_{j=1}^{5}(F_{j,\max}^{-}/\Delta_{j,\max}^{-}) \quad (3)$$

where $\Delta_{j,\max}$ is the measured maximum lateral displacement and $F_{j,\max}$ is the corresponding lateral load within a cycle at displacement Δ. The superscripts + and – denote the values obtained at the positive and negative directions, respectively.

Figure 14 shows the degradation of secant stiffness K_{Δ} versus the lateral displacement Δ for the original and repaired pier specimens. A close examination of these plots indicates that the pier repair has influenced the rate of stiffness degradation. At the early stage of lateral displacement loading, all the repaired specimens exhibit lower lateral stiffness due to the reasons discussed previously. However, all the repaired specimens show a slower rate of stiffness degradation than the original ones. And at later stages of the tests, all the repaired specimens show a higher lateral stiffness than the original ones.

3.4 Energy dissipating capacity

The energy dissipation, which is calculated as the area enclosed by a hysteretic loop, is commonly used to quantify the seismic energy absorption ability of RC structures. The cumulative energy E_{Δ} versus the top displacement Δ for the original and repaired pier specimens is shown in Fig. 15 and compared with each other. Generally speaking, each pair of specimens exhibits no noticeable difference with regard to their energy dissipation capacity. Specimen A10-R shows a larger cumulative energy when the top displacements are between 30 and 60 mm. However, the cumulative energy dissipated by specimen A10 is slightly larger than specimen A10-R when the top displacement reaches 90 mm. The cumulative energies dissipated by specimens A12 and A12-R are almost the same before the top displacement reaches 60 mm. However, specimen A12-R shows a larger cumulative energy than specimen A12 when the top displacement reaches 80 mm. For specimens A14 and A14-R, the repaired specimen shows a slightly lower cumulative energy than the original one during all the testing phases.

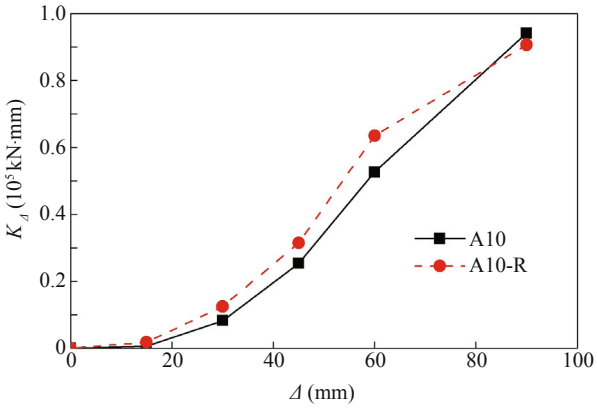

(a) Specimens A10 and A10-R

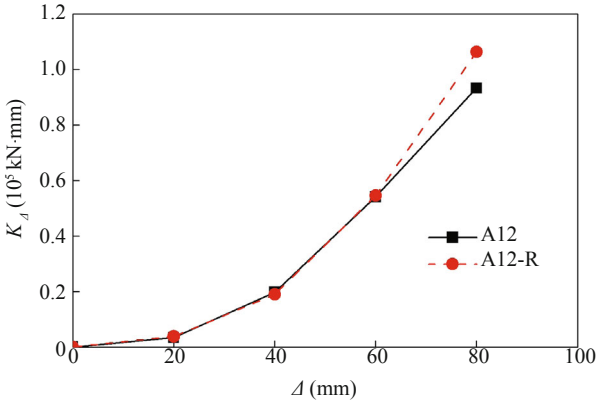

(b) Specimens A10 and A10-R

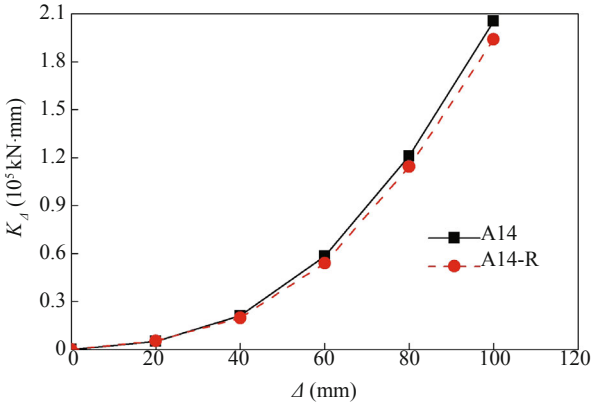

(c) Specimens A14 and A14-R

Fig. 15 Cumulative energy versus top displacement for the specimens

3.5 Strains in the CFRP sheets

To better understand of the confining effect of the CFRP, strains of the CFRP sheets in the circumferential direction of the repaired specimens at different loading levels are measured and shown in Fig. 16. It can be seen that the maximum strain measured in specimen A14-R is about 0.00392, which is in good agreement with the strain limit of 0.004 suggested by Priestley and Seible (1995) and used in current seismic retrofit design practice (Ozbakkaloglu and Saatcioglu, 2006).

In the literature, there are some other studies (Sun *et al*., 2011; Vosooghi and Saiidi, 2013a; Lavorato and Nuti, 2015) in which the strain of the CFRP sheets used to repair the circular pier specimens is measured. For example, quasi-static tests conducted by Sun *et al*. (2011) indicated that the maximum measured CFRP strains were between 0.003 and 0.00942 for different pier specimens. The shake table tests conducted by Vosooghi and Saiidi (2013a) indicated that the maximum CFRP strains were between 0.003597 and 0.00941. And the pseudo-dynamic tests conducted by Lavorato and Nuti (2015) revealed that the maximum measured CFRP strain was about 0.003. Many parameters, such as the specimen aspect ratio, specimen axial load ratio, cross section shape and dimension, repair technique and material, and the loading sequence, may influence the measured CFRP strain. As a result, it is very difficult to give an estimate

of the ultimate CFRP strain for pier repair design. Note that in most cases, the recorded CFRP strain seems to fit the recommended value of 0.004 for seismic retrofit design practice (Ozbakkaloglu and Saatcioglu, 2006). A design strain of 0.004 for CFRP sheets can therefore be used for pier repair design until more effective test results are available.

As for specimen A10-R, it is seen that the maximum strain of the CFRP sheets is only 0.0008, which is much less than that in specimen A14-R, indicating that the confining effect of the CFRP sheets in specimen A10-R is limited and the CFRP sheets did not play an obvious role in restoration of the behavior of the repaired specimen.

4 Evaluation of the design equation for required CFRP thickness

Based on an analysis of the shaking table test results of repaired circular RC bridge piers using CFRP, Vosooghi and Saiidi (2013b) proposed design guidelines for the repair of earthquake-damaged bridge piers. For a circular earthquake-damaged bridge pier with the flexural failure mode, the required CFRP jacket thickness can be calculated as follows:

$$t_j = \frac{f_l D}{2E_j \varepsilon_j} \tag{4}$$

where t_j is the CFRP jacket thickness, f_l is the required confinement pressure, which can be taken as 2069 kPa for severely earthquake-damaged piers, D is the CFRP confined pier diameter, E_j is the CFRP modulus of elasticity and ε_j is the jacket nominal design strain of 0.004. Note that the required confinement pressure of 2069 kPa was recommended based on the measured CFRP strain during the pseudo-dynamic tests on the repaired pier specimens. And the repaired specimen was assumed to fail at a displacement ductility factor of 5. Moreover, a nominal design strain of 0.004 for the CFRP and a safety factor of 0.9 were considered, as discussed by Vosooghi and Saiidi (2013b).

Until recently, experimental studies on the seismic repair of circular bridge piers have been very limited. In this study, a total of four circular pier specimens that failed due to flexural failure mode and repaired with CFRP sheets are collected to evaluate the efficiency of Eq. (4). The collected test data contain specimen A14-R from the present study, and P-type, SE-type and E-type specimens tested by Youm *et al.* (2006). All the repaired specimens perform well and the deformation capacity of the repaired specimens is higher than that of the original ones. The actually used CFRP thickness of all the specimens are compared with Eq. (4) and listed in Table 3. It was found that except for specimen A14-R in the present study, all the other specimens use almost the same CFRP thickness as recommended by Eq. (4). Specimen A14-R is repaired with fewer CFRP sheets when compared with Eq. (4), and the repaired specimen exhibits a good seismic behavior, as discussed in the previous section. By a close examination of all the specimens listed in Table 3, it is found that all the specimens except for A14-R are repaired with the same cross-section, while the repaired section of the specimen A14-R is enlarged.

As shown in Fig. 16(b), the maximum measured CFRP strain is 0.00392, corresponding to a stress of 960.4 MPa (obtained by multiplying the strain of 0.00392 by the modulus of elasticity of 245 GPa). Using the calculated stress of the CFRP sheets, the confinement pressure f_l provided by the CFRP sheets is calculated as follows:

$$f_l = \frac{2f_j t_j}{D} \tag{5}$$

where f_j is the stress of the CFRP sheet.

The maximum confinement pressure obtained from Eq. (5) for specimen A14-R is 853 kPa, which is much less than the value (2069 kPa) suggested by Vosooghi and Saiidi (2013b). Note that although the maximum measured CFRP strain in specimen A14-R agrees well with the design strain of 0.004, the CFRP jacket thickness t_j in specimen A14-R is much less than that used in the specimens conducted by Vosooghi and Saiidi (2013b). As a result, the confinement pressure f_l of specimen A14-R is much less than the value suggested by Vosooghi and Saiidi (2013b). The lower confinement pressure indicates that for a pier specimen repaired with an enlarged cross-section, the needed thickness of the CFRP sheets can be reduced significantly compared with the values suggested by Vosooghi and Saiidi (2013b).

5 Numerical modelling of the repaired specimens

The pre-existing damage in the concrete and reinforcement bars makes it difficult to predict the response of repaired RC structures. In the present study, a finite element model to predict the cyclic behavior of the repaired pier specimens is developed and calibrated with the test results. The model is built based on a general finite element analysis program called OpenSees (Mazzoni *et al*., 2006).

As specimen A12-R is damaged as a result of the debonding failure of the concrete jacket, this repair technique is not recommended in engineering practice. Cyclic analysis is conducted for specimens A10-R and A14-R. Note that both specimens A10-R and A14-R failed with a ductile flexural mode, and the quasi-static tests conducted by Lehman (1998) indicate that the contribution of the shear deformation to the total lateral displacement is less than 5% for piers with an aspect ratio larger than 4. Even for specimen A10-R with reduced effective height, the aspect ratio is 4.875 (effective height of 1950 mm divided by the section diameter of 400 mm). As a result, only flexural and longitudinal bar

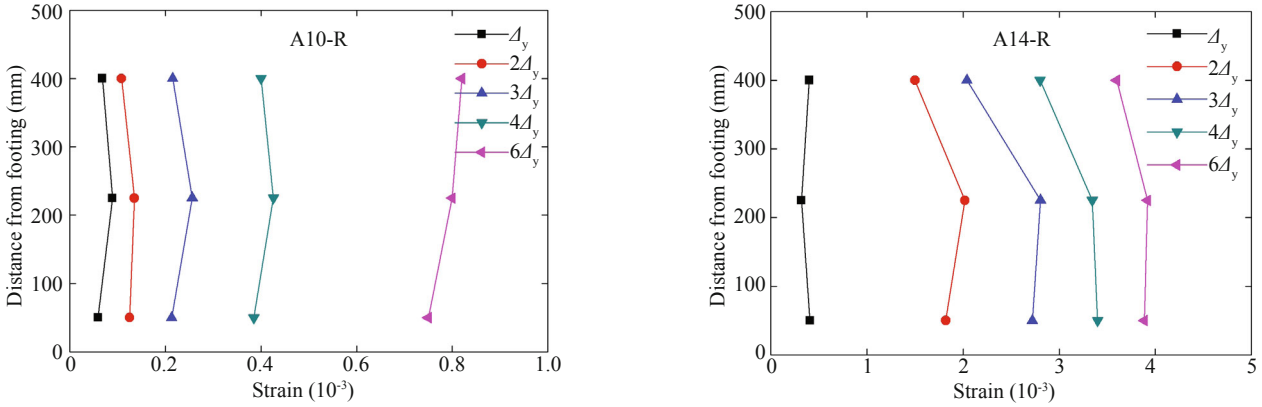

(a) Specimens A10-R (b) Specimens A14-R

Fig. 16 Measured CFRP strains

Table 3 Test data for repaired circular pier specimens using CFRP

Specimen	CFRP thickness (mm)		Deformation capacity DR (%)	
	Calculated by Eq. (4)	Actually used in the test	Original	Repaired
A14-R	0.53	0.222	4.2	> 4.2
P-type	0.34	0.33	> 8.0	> 8.0
SE-type	0.34	0.33	> 6.0	> 8.0
E-type	0.34	0.33	4.5	> 8.0

Note: DR is the ultimate drift ratio of the specimen, defined as the measured maximum lateral displacement divided by the pier height.

slip deformations are considered and deformation due to shear is neglected in the present model (Saiidi and Cheng, 2004).

Figure 17 shows the finite element models for specimens A10-R and A14-R. Note that due to the large size, strength and stiffness of the RC footing, it is not modeled and only the specimen above the footing top is considered. The total lateral response of each specimen is modeled by coupling flexural and longitudinal bar slip responses by two kinds of elements in series, where the force in each element is the same and the total lateral deformation is the summation of each individual element deformation. The flexural deformation is modeled by the nonlinear beam-column element, while the longitudinal bar slip deformation is modeled by the zero-length fiber section element. For each specimen, two nonlinear beam-column elements are used to model the flexural deformations of the repaired region and the specimen above the repaired region, respectively. The slip of the longitudinal bar from the RC footing is modeled by a zero-length section element.

The nonlinear beam-column element used in the present study accounts for the nonlinear flexural deformation by assuming that the plane sections remain plane and captures the spread of plasticity along the element. The nonlinear hysteretic behavior of the element is derived from the constitutive relations of concrete and reinforcing steel fibers into which each section is divided. All concrete fibers are modeled by using the "Concrete 01" uniaxial material model in OpenSees, which is based on the modified Kent and Park concrete model. Longitudinal bars are modeled using "Steel 02", which is based on the Giuffre-Menegotto-Pinto model. The "Steel 02" material model is able to reproduce the Bauschinger effect of the longitudinal bar under cyclic load, while the buckling damage is not considered. Note that some cyclic stress-strain models for reinforcing bars including buckling damage (Monti and Nuti, 1992; Gomes and Appleton, 1997; Dhakal and Maekawa, 2002) have been proposed. The buckling damage model is not considered in the present study though the accuracy of the simulation result might be further improved when the buckling damage model is considered.

It is known that the elastic modulus of the longitudinal bars will be reduced under the cyclic loading, which makes it is essential to consider the pre-existing damage in the longitudinal bars of the repaired specimens. In this study, a modified steel material model is used to account for the damage to the longitudinal bars. The initial elastic modulus E_0 of the longitudinal bars is modified to account for the pre-existing damage, and the modification factor γ varies depending on the damage state. Here, γ is taken as 0.3 (E_0 = 60 kN/mm^2) for the buckled longitudinal bars in the repaired region, and γ changes to 0.5 (E_0 = 100 kN/mm^2) for other longitudinal bars in the repaired region. Obviously, the elastic modulus for the additional longitudinal bars should not be modified (γ is taken as 1.0). For the longitudinal bars above the repaired region, γ is taken as 0.9 (E_0 = 180 kN/mm^2). Also, note that the yield strength of all the longitudinal bars is taken as the same value as in the original pier specimens.

The "Concrete 01" material model is used to represent the stress-strain relationship of concrete in compression while the tensile strength is neglected. For the concrete

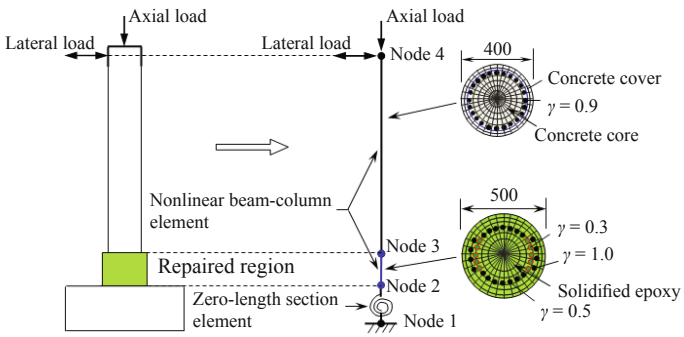

(a) Specimens A10-R

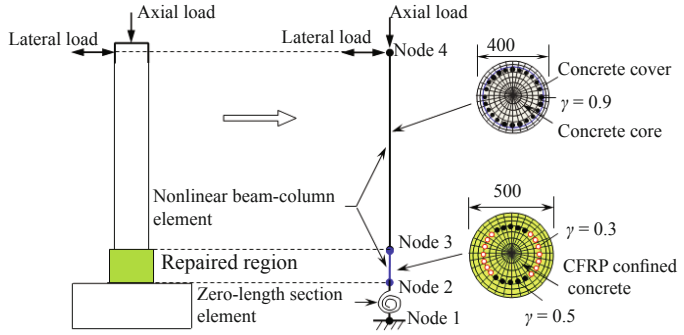

(b) Specimens A14-R

Fig. 17 Numerical model of the repaired specimens

above the repaired region, the concrete strain ε_0 at maximum strength is enlarged (taken as 0.004–0.005) to account for the pre-existing damage in the concrete, while the compression strength of the cover concrete is taken as the same value as in the original specimen. By using this assumption, the compression modulus of the concrete can be reduced to account for the pre-existing damage. The strength of the concrete core is enhanced to account for the confining effect provided by the spiral bars. As the solidified epoxy in the repaired region of specimen A10-R is within the elastic range during the test, the epoxy is modeled by an elastic material model. For specimen A14-R, the concrete property in the repaired region is adjusted to account for the confining effect of the CFRP sheets, while the confinement effect of the spiral bars is neglected (Vosooghi and Saiidi, 2013b). The model proposed by Saiidi *et al*. (2005) is used to determine the ultimate strain and corresponding stress of the CFRP confined concrete.

The longitudinal bar slip deformation results from the extension of the longitudinal bar from the RC footing, and this deformation is modeled by a zero-length fiber section element (Ghannoum and Moehle, 2012). The section of the element has the same geometry as the fiber section of the beam-column element it is attached to but with different material properties for its steel and concrete fibers. For the steel fiber, the constitutive law of the steel reinforcement is modified from a stress-strain relation to a stress-slip relation. For concrete fiber in the fiber section element, the "Concrete 01" uniaxial material model is also used as in the beam-column element. While the concrete strain at the maximum stress is multiplied by a scale factor (taken as 10-20) to maintain compatibility between the beam-column element and the bar slip section element (Ghannoum, 2007).

Both the axial load and lateral displacement history adopted in the tests are applied to the analysis model. The simulated hysteretic curves for both specimens are compared with the test results, and are shown in Fig. 18. The results indicate that by the proposed numerical analysis model, the simulated lateral load-displacement hysteretic curves of the repaired specimens agree well with the tested curves. Both the simulated initial lateral stiffness and the lateral strength closely match the test results. A close examination of Fig. 18 indicates some differences between the simulated and tested hysteretic curves. First, the simulated residual displacement (measured when the lateral load is zero) for both of the specimens is less than the corresponding test result. Second, no strength degradation is observed in the simulated hysteretic curve of specimen A14-R and the failure of this specimen could not be predicted. The reason for the differences between the simulated and test results may be attributed to two aspects: (a) the modification factor γ for the initial elastic modulus of the longitudinal bar is only a simple method to account for the existing damage, while the low initial elastic modulus of the longitudinal bar leads

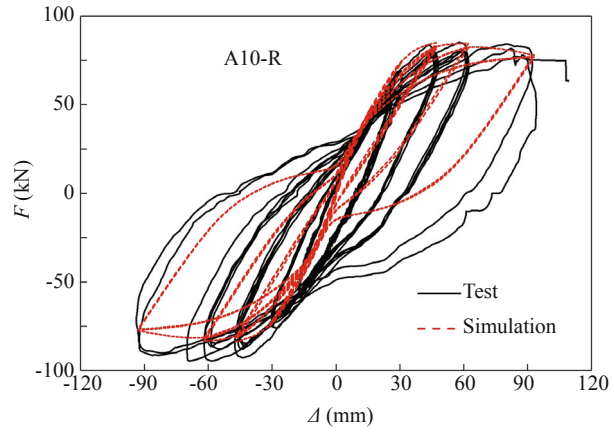

(a) Specimens A10-R

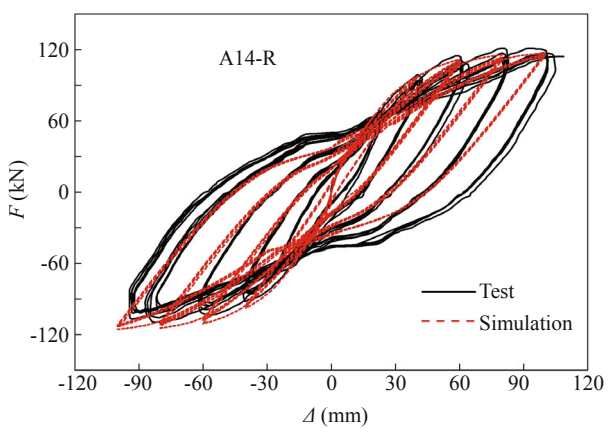

(b) Specimens A14-R

Fig. 18 Comparison of the hysteretic curves between simulated and tested results

to a small residual displacement; and (b) the buckling damage of the longitudinal bar is not considered in the proposed model, which results in a high lateral strength at later stage of testing.

6 Conclusions

Three original circular pier specimens are designed and severely damaged with a ductile flexural failure mode under cyclic lateral force and constant axial load. Three different rapid repair techniques are proposed to repair the damaged specimens within four days by using the early-strength concrete jacket, additional longitudinal bars, epoxy, and CFRP sheets. The repaired specimens are retested under the same axial and lateral loads and the results are compared with the original ones. The design equation for the needed CFRP thickness proposed by Vosooghi and Saiidi (2013b) is evaluated by comparing it with available test data. Finally, a finite element model to predict the cyclic behavior of the repaired specimens is presented and the numerical results are compared with the test data. Some conclusions are drawn as follows:

(1) All the repaired specimens exhibit a larger deformation capacity than the original ones. For the specimen repaired using an epoxy jacket, the new flexural plastic hinge moves from the base of the pier to the portion just above the top of the repaired region and no obvious failure is observed in the repaired region. The phenomenon obviously exhibits greater lateral strength than the original one. The measured maximum strains in both the additional longitudinal bars and the wrapped CFRP sheets are very limited, indicating both the additional bars and the CFRP sheets did not play an obvious role in restoring the behavior of the repaired specimen.

(2) For the specimen repaired with the early-strength concrete jacket and additional longitudinal bars, the maximum lateral strength is 1.15 times larger than the original one in the positive direction and almost the same in the negative direction. The early-strength concrete jacket exhibits a high brittle behavior for lack of confinement, and debonding failure occurs between the new concrete jacket and existing old concrete. The additional longitudinal bars are not effective in enhancing the behavior of the repaired specimen. As a result, the early-strength concrete jacket without FRP confinement or interface treatment is not recommended for repair of earthquake-damaged bridge piers.

(3) The specimen repaired with the early-strength concrete jacket wrapped by the CFRP sheets exhibits similar or larger lateral strength when compared to the original one. At the end of the test, no apparent plastic hinge is formed and the failure pattern is dominated by flexural cracks on the CFRP sheets along the fiber direction. No tension failure of the CFRP fibers is observed.

(4) The initial lateral stiffness of all the repaired specimens is lower than that of the original ones as a result of the pre-existing damage in the tested specimens. However, a slower rate of stiffness degradation is observed for the repaired specimens than the original ones. At the later stages of the tests, all the repaired specimens show a higher lateral stiffness than that of the original ones. No noticeable difference is observed for the energy dissipation capacity between the original and repaired piers for all the specimens.

(5) For circular bridge piers repaired without an enlarged cross section, the needed CFRP jacket thickness can be obtained by the design equation proposed by Vosooghi and Saiidi (2013b). While for piers repaired with an enlarged cross-section, the needed CFRP jacket thickness can be reduced.

(6) The proposed finite element model based on the nonlinear beam-column element and zero-length section element considering the pre-existing damage in the longitudinal bar and concrete could be used to predict the cyclic behavior of the repaired pier specimens.

(7) Since the cost of the epoxy is expensive when compared to concrete, it is suggested that the repair technique using the early-strength concrete jacket confined by the CFRP sheets can be an optimal one for the rapid repair of severely earthquake-damaged circular bridge piers with flexural failure mode.

Acknowledgement

The authors gratefully acknowledge the support for this research by the National Natural Science Foundation of China under Grant No. 51678150; Science for Earthquake Resilience under Grant No. XH17064; The third author acknowledge the partial support from Australian Research Council Discovery Early Career Researcher Award (DECRA).

References

Aboutaha RS, Engelhardt MD, Jirsa JO and Kerger ME (1999), "Experimental Investigation of Seismic Repair of Lap Splice Failures in Damaged Concrete Columns," *ACI Structural Journal*, **96**(2): 297–307.

Chang SY, Li YF and Loh CH (2004), "Experimental Study of Seismic Behaviors of As-built and Carbon Fiber Reinforced Plastics Repaired Reinforced Concrete Bridge Columns," *Journal of Bridge Engineering*, ASCE, **9**(4): 391–402.

Cheng CT, Yang JC, Yeh YK and Chen SE (2003), "Seismic Performance of Repaired Hollow-bridge Piers," *Construction and Building Materials*, 2003, **17**(5): 339–351.

Dhakal RP and Maekawa K (2002), "Modeling for Postyield Buckling of Reinforcement," *Journal of Structural Engineering*, ASCE, **128**(9): 1139–1147.

Fakharifar M, Chen G, Sneed L and Dalvand A (2015), "Seismic Performance of Post-mainshock FRP/Steel Repaired RC Bridge Columns Subjected to Aftershocks," *Composites*: *Part B*, **72**: 183–198.

Frangou M, Pilakoutas K and Dritsos S (1995), "Structural Repair/Strengthening of RC Columns," *Construction and Building Materials*, **9**(5): 259–266.

Fukuyama K, Higashibata Y and Miyauchi Y (2000), "Studies on Repair and Strengthening Methods of Damaged Reinforced Concrete Columns," *Cement & Concrete Composites*, **22**(1): 81–88.

GB 50367-2006 (2006), *Design Code for Strengthening Concrete Structure*, Beijing: China Architecture & Building Press. (in Chinese)

Ghannoum WM (2007), "Experimental and Analytical Dynamic Collapse Study of a Reinforced Concrete Frame with Light Transverse Reinforcement," *Doctoral Thesis*, Berkeley: University of California, Berkeley.

Ghannoum WM and Moehle JP (2012), "Dynamic Collapse Analysis of a Concrete Frame Sustaining Column Axial Failures," *ACI Structural Journal*, 2012, **109**(3): 403–412.

Gomes A and Appleton J (1997), "Nonlinear Cyclic Stress-strain Relationship of Reinforcing Bars Including Buckling," *Engineering Structures*, **19**(10): 822–826.

He R, Grelle S, Sneed LH and Belarbi A (2013a), "Rapid Repair of a Severely Damaged RC Column Having Fractured Bars Using Externally Bonded CFRP," *Composite Structures*, **101**: 225–242.

He R, Sneed LH and Belarbi A (2013b), "Rapid Repair of Severely Damaged RC Columns with Different Damage Conditions: An Experimental Study," *International Journal of Concrete Structures and Materials*, **7**(1): 35–50.

Hose Y, Silva P and Seible F (2000), "Development of a Performance Evaluation Database for Concrete Bridge Components and Systems under Simulated Seismic Loads," *Earthquake Spectra*, **16**(2): 413–442.

JTG/T B02-01 2008 (2008), *Guidelines for Seismic Design of Highway Bridges*, Beijing: China Communications Press. (in Chinese)

Júlio ENBS and Branco AB (2008), "Reinforced Concrete Jacketing-interface Influence on Cyclic Loading Response," *ACI Structural Journal*, **105**(4): 471–477.

Júlio ENBS, Branco AB and Silva VD (2005), "Reinforced Concrete Jacketing-interface Influence on Monotonic Loading Response," *ACI Structural Journal*, **102**(2): 252–257.

Kim SH and Choi JH (2010), "Repair of Earthquake-damaged RC Columns with Stainless Steel Wire Mesh Composite," *Advances in Structural Engineering*, **13**(2): 393–401.

Lavorato D and Nuti C (2015), "Pseudo-dynamic Tests on Reinforced Concrete Bridges Repaired and Retrofitted after Seismic Damage," *Engineering Structures*, **94**: 96–112.

Lehman DE (1998), "Seismic Performance of Well-confined Concrete Bridge Columns," *Doctoral Thesis*, Berkeley: University of California, Berkeley.

Lehman DE, Gookin SE, Nacamuli AM and Moehle JP (2001), "Repair of Earthquake-damaged Bridge Columns," *ACI Structural Journal*, **98**(2): 233–242.

Li YF and Sung YY (2003), "Seismic Repair and Rehabilitation of a Shear-failure Damaged Circular Bridge Column Using Carbon Fiber Reinforced Plastic Jacketing," *Canadian Journal of Civil Engineering*, **30**(5): 819–829.

Lu Y, Vintzileou E, Zhang GF and Tassios TP (1999), "Reinforced Concrete Scaled Columns under Cyclic Actions," *Soil Dynamics and Earthquake Engineering*, **18**(2): 151–167.

Mazzoni S, McKenna F, Scott MH and Fenves GL (2006), *OpenSees Command Language Manual*, Pacific Earthquake Engineering Research Center, University of California, Berkeley, Richmond, California, USA.

Monti G and Nuti C (1992), "Nonlinear Cyclic Behavior of Reinforcing Bars Including Buckling," *Journal of Structural Engineering*, ASCE, **118**(12): 3268–3284.

Ozbakkaloglu T and Saatcioglu M (2006), "Seismic Behavior of High-strength Concrete Columns Confined by Fiber-reinforced Polymer Tubes," *Journal of Composites for Construction*, ASCE, **10**(6): 538–549.

Ozcelik R, Akpınar U and Binici B (2011), "Seismic Retrofit of Deficient RC Structures with Internal Steel Frames," *Advances in Structural Engineering*, **14**(6): 1205–1222.

Priestley MJN and Seible F (1995), "Design of Seismic Retrofit Measures for Concrete and Masonry Structures," *Construction and Building Materials*, **9**(6): 365–377.

Rutledge ST, Kowalsky MJ, Seracino R and Nau JM (2014), "Repair of Reinforced Concrete Bridge Columns Containing Buckled and Fractured Reinforcement by Plastic Hinge Relocation," *Journal of Bridge Engineering*, ASCE, **19**(8): A4013001-1-A4013001-10.

Saadatmanesh H, Ehsani MR and Jin L (1997), "Repair of Earthquake-damaged RC Columns with FRP Wraps," *ACI Structural Journal*, **94**(2): 206–215.

Saiidi MS and Cheng Z (2004), "Effectiveness of Composites in Earthquake-damage Repair of Reinforced Concrete Flared Columns," *Journal of Composites for Construction*, ASCE, **8**(4): 306–314.

Saiidi MS, Sureshkumar K and Pulido C (2005), "Simple Carbon-fiber-reinforced-plastic-confined Concrete Model for Moment-curvature Analysis," *Journal of Composites for Construction*, ASCE, **9**(1): 101–104.

Shin M and Andrawes B (2011), "Emergency Repair of Severely Damaged Reinforced Concrete Columns Using Active Confinement with Shape Memory Alloys," *Smart Materials and Structures*, **20**(6): 1–9.

Si BJ, Sun ZG, Wang QX and Wang DS (2010), "Research on Rapid Repair Techniques for Earthquake-damaged Ductile RC Bridge Piers," *Journal of Dalian University of Technology*, **50**(1): 93–98. (in Chinese)

Sun ZG, Wang DS, Du XL and Si BJ (2011), "Rapid Repair of Severely Earthquake-damaged Bridge Piers with Flexural-shear Failure Mode," *Earthquake Engineering and Engineering Vibration*, **10**(4): 553–567.

Sun ZG, Wang DS, Guo X, Si BJ and Huo Y (2012), "Lessons Learned from the Damaged Huilan Interchange in the 2008 Wenchuan Earthquake," *Journal of Bridge Engineering*, ASCE, **17**(1): 15–24.

Vosooghi A and Saiidi MS (2013a), "Shake-table Studies of Repaired Reinforced Concrete Bridge Columns Using Carbon Fiber-reinforced Polymer Fabrics," *ACI Structural Journal*, **110**(1): 105–114.

Vosooghi A and Saiidi MS (2013b), "Design Guidelines for Rapid Repair of Earthquake-damaged Circular RC Bridge Columns Using CFRP," *Journal of Bridge Engineering*, ASCE, **18**(9): 827–836.

Wang DS, Li HN, Zhao YH, and Wang GX (2006), "Displacement-based Seismic Design Method of RC Bridge Piers," *China Civil Engineering Journal*, **39**(10): 80–86. (in Chinese)

Wang XY (2010), "Seismic Response Analysis of Huilan Ramp Bridge in Mianzhu," *Master Thesis*, Chengdu: Southwest Jiaotong University. (in Chinese)

Xiao Y and Ma R (1997), "Seismic Retrofit of RC Circular Columns Using Prefabricated Composite Jacketing," *Journal of Structural Engineering*, ASCE, **123**(10): 1357–1364.

Yang Y, Sneed LH, Morgan A, Saiidi MS and Belarbi A (2015a), "Repair of RC Bridge Columns with Interlocking Spirals and Fractured Longitudinal Bars – An Experimental Study," *Construction and Building Materials*, **78**: 405–420.

Yang Y, Sneed LH, Saiidi MS, Belarbi A, Ehsani M, and He R (2015b), "Emergency Repair of an RC Bridge Column with Fractured Bars Using Externally Bonded Prefabricated Thin CFRP Laminates and CFRP Strips," *Composite Structures*, **133**: 727–738.

Yilmaz S, Özen MA and Yardim Y (2013), "Tensile Behavior of Post-installed Chemical Anchors Embedded to Low Strength Concrete," *Construction and Building Materials*, **47**: 861–866.

Youm KS, Lee HE and Choi S (2006), "Seismic Performance of Repaired RC Columns," *Magazine of Concrete Research*, **58**(5): 267–276.